ELSEVIER

Atmospheric Research 38 (1995) 29–62

ATMOSPHERIC RESEARCH

New RAMS cloud microphysics parameterization Part I: the single-moment scheme

R.L. Walko, W.R. Cotton *, M.P. Meyers, J.Y. Harrington

Colorado State University, Department of Atmospheric Science, Fort Collins, CO 80523, USA

Accepted 4 November 1994

Abstract

A new cloud microphysical parameterization is described. Features of this new scheme include: the use of generalized gamma distributions as the basis function for all hydrometeor species; the use of a heat budget equation for hydrometeor classes, allowing heat storage and mixed phase hydrometeors; partitioning hydrometeors into seven classes (including separate graupel and hail categories); the use of stochastic collection rather than continuous accretion approximations and extension of the ice nucleation scheme to include homogeneous nucleation of ice from haze particles and cloud droplets.

The versatility and credibility of the new scheme is explored, using sensitivity experiments for a simple two-dimensional convective cloud simulation.

1. Introduction

In this paper we describe a new cloud microphysics parameterization that has been introduced into the Regional Atmospheric Modeling System (RAMS) developed at Colorado State University. It is appropriate that we present the newest version of the cloud microphysics scheme developed under the direction of William R. Cotton (hereafter referred to as WRC) in this Helmut Weickmann memorial volume. The first microphysics scheme developed by WRC was supported by ESSA Contract No. E22-103-68 (N) (see Lavoie et al., 1970; later published in Cotton, 1972a, b) for investigations of lake effect storms. Helmut, who served as the program manager of the project, was particularly interested in that earlier scheme and often discussed its physical basis and approximations in detail with WRC. That early scheme subdivided hydrometeor species into four components, cloud droplets, raindrops, frozen hydrometeors and pristine ice crystals. Pristine ice crystals had a mono-disperse size-spectrum but, in addition to crystal mass, the bulk geometry of the

* Corresponding author.

SSDI 0169-8095(94)00087-5

crystals (a-axis and c-axis) was predicted and stored. Like almost all microphysics parameterizations of the time (Weinstein and Davis, 1968; Simpson and Wiggert, 1969; Weinstein, 1970; Wisner et al., 1972; Koenig, 1977; Orville and Kopp, 1977), the first scheme followed the lead of Kessler (1969), in which the size-spectra of the other hydrometeor classes was assumed to be Marshall and Palmer (1948) with the intercept parameter N_o specified by the user. Also, all collection equations were approximated by continuous collection solutions.

Later Cotton et al. (1982, 1986) introduced a scheme in the predecessor numerical prediction cloud model to RAMS, that included an ice crystal class that was greatly simplified over the older scheme since it was too computationally expensive to keep track of ice crystal geometry. Moreover, the original Marshall and Palmer exponential size-spectra used by Kessler was modified somewhat to include a user-specified constant slope given by a constant characteristic diameter rather than a constant N_o.

Almost all the earlier microphysics parameterization schemes involved prediction of a single moment of the hydrometeor size-spectra, namely the mass mixing ratio of the species which is proportional to the third moment. There is a trend in recent years to extend those earlier bulk microphysical schemes to include predictions on an additional moment of the spectrum, namely the concentration of the species (e.g., Nickerson et al., 1978, Nickerson et al., 1986; Ziegler, 1985; Ferrier, 1993; Wang and Chang, 1993). In this paper, which we shall call Part I, we describe the new scheme in RAMS that includes several new features. These include the use of a generalized gamma size-spectrum, rather than only a Marshall–Palmer spectrum, the introduction of ice–liquid mixed phase hydrometeor categories, a double moment spectrum for ice crystals, and new heterogeneous and homogeneous nucleation parameterizations. In addition, approximate solutions to the stochastic collection equation based on Verlinde et al. (1990) are used rather than the continuous accretion approximation. Furthermore, thermal equilibrium is not assumed for the rain, graupel and hail hydrometeor classes. In Meyers et al. (1994; hereafter referred to Part II) we describe the extension of the scheme to prediction on hydrometeor concentration, in addition to mass mixing ratio.

2. Model formulation

2.1. Categories of water

Water is categorized in up to eight forms: vapor, cloud droplets, rain, pristine ice, snow, aggregates, graupel and hail. Cloud droplets and rain are liquid water, but may be supercooled. Pristine ice, snow and aggregates are assumed to be completely frozen, while graupel and hail are mixed-phase categories, capable of consisting of ice only or a mixture of ice and liquid.

Cloud droplets are assumed small enough to not fall, while all other categories do fall. Cloud droplets and pristine ice are the only categories to nucleate from vapor. All other categories form from existing hydrometeors, but once formed, may also grow by vapor deposition. Pristine ice may also continue its growth by vapor deposition, and is not permitted to grow by any other process. The definition of the pristine ice category is restricted

to relatively small crystals, and larger pristine ice crystals are categorized as snow. The snow category is defined here as consisting of relatively large ice crystals which have grown by vapor deposition and riming. Together, the pristine ice and snow categories allow a bimodal representation of ice crystals. Aggregates are defined as ice particles that have formed by collision and coalescence of pristine ice, snow, and/or other aggregates. Like snow, aggregates are allowed to retain their identity with moderate amounts of riming. Pristine ice, snow and aggregates are all low-density ice particles, having relatively low mass and fall speed for their diameters. Graupel is an intermediate density hydrometeor. It is assumed to be approximately spherical in shape, and to be formed by moderate to heavy riming and/or partial melting of pristine ice, snow or aggregates. Graupel is allowed to carry up to only a low percentage of liquid. If the percentage becomes larger, by either melting or riming, a graupel particle is re-categorized as hail. Hail is a high-density hydrometeor, considered spherical in shape. It is assumed to be formed by freezing of rain drops or by riming or partial melting of graupel. Hail is allowed to carry any fraction of liquid water up to, but not including, 100%, except that all but small hail will shed excessive liquid.

Note that these definitions of graupel and hail emphasize their composition and density more than their method of formation. For example, a snowflake or aggregate undergoing gradual melting in this scheme first converts to graupel, then to hail, and finally to rain, although hail is usually thought of as forming from riming of supercooled water onto an ice nucleus or from freezing of supercooled rain. One purpose of this approach is to more accurately model a hydrometeor's fall velocity and consequent rates of ventilation and collision as it undergoes transformation to different densities. As will be discussed, fall velocity is a function of diameter and category only, so changing categories is the means for changing the velocity of a given diameter particle. Another purpose, regarding transferring mostly melted ice to the hail category, is that if re-freezing happens to occur, the result should be hail rather than low-density ice or supercooled rain. Other criteria for categorization are possible, including a size distinction between graupel and hail following some definitions of the two. These are being explored elsewhere with the new model, but are not a part of the present work.

2.2. *Hydrometeor size distributions and power laws*

Hydrometeors in each category are assumed to conform to a generalized gamma distribution described by Flatau et al. (1989) and Verlinde et al. (1990), given by

$$f_{gam}(D) = \frac{1}{\Gamma(\nu)} \left(\frac{D}{D_n}\right)^{\nu-1} \frac{1}{D_n} \exp\left(-\frac{D}{D_n}\right), \tag{1}$$

where hydrometeor diameter D may range from zero to infinity, and $\Gamma(\nu)$ is a normalization constant making the integral over D from zero to infinity of f_{gam} equal to 1. Other symbols are defined in Table 1. The number density distribution is described by

$$n(D) = N_t f_{\text{gam}}(D), \tag{2}$$

where N_t is the total concentration of the category. The shape parameter ν may be any real number greater than or equal to 1, and controls the relative amount of smaller vs. larger hydrometeors in the distribution. For example, when $\nu = 1$, Eq. (1) reduces to the expo-

Table 1
Nomenclature

B	quantity defined by Eq. (31) (dimensionless)
C	quantity defined by Eq. (34) ($m\ s\ kg^{-1}$)
C_i, C_l	specific heats of ice and liquid water ($J\ kg^{-1}\ K^{-1}$)
C_p	specific heat of air at constant pressure ($J\ kg^{-1}\ K^{-1}$)
D	diameter of an individual hydrometeor (m)
D_b	diameter that separates the pristine ice and snow categories (m)
$D_{\overline{m}}$	diameter of hydrometeor whose mass is $\overline{m}$ (m)
D_{mean}	mean diameter of a category (m)
D_{mode}	modal diameter of a category (m)
D_n	characteristic diameter of modified gamma distribution (m)
$e_{s\ell}$	saturation vapor pressure over liquid (Pa)
E	collection efficiency (dimensionless)
f_{gam}	probability density function for modified gamma distribution, or fraction of hydrometeors of a given category per unit increment of diameter D occurring at D (m^{-1})
f_{nuc}	fraction of haze particles which freeze homogeneously in 1 s (dimensionless)
f_{Re}	ventilation coefficient for a hydrometeor (dimensionless)
F_e	function giving the fraction of pristine ice crystal concentration sublimated in a timestep (dimensionless)
F_{Re}	mean value of ($D f_{Re}$) integrated over a category size distribution (m)
F_ρ	fall speed adjustment dependent on air density (dimensionless)
$F1$,$F2$,f_t	expressions defined in Eqs. (55–57) for contact nucleation
H	habit of pristine ice (dimensionless)
i_g, i_h	fractional amounts of ice in graupel and hail categories (dimensionless)
J	collection table value ($kg\ m^3\ s^{-1}$)
K_n	Knudson number (dimensionless)
$L_{\ell v}$, L_{iv}, $L_{i\ell}$	latent heats of evaporation, sublimation, and melting ($J\ kg^{-1}$)
m	mass of an individual hydrometeor (kg)
$\overline{m}$	mean value of m over a category size distribution (kg)
m_l, m_i	m_l is liquid water mass shed from a hail particle containing ice mass m_i (kg)
m_n	initial mass of nucleated ice crystal (kg)
$n(D)$	number of hydrometeors of a given category per cubic meter per unit increment of diameter D occurring at D (m^{-4})
N_a	concentration of ice nuclei available for contact freezing (m^{-3})
N_h	concentration of haze particles (m^{-3})
N_t	number concentration of hydrometeors of a given category (m^{-3})
N_{tc}	cloud droplet concentration (m^{-3})
N_0	Marshall – Palmer y-intercept concentration of a category (m^{-4})
$(N_t)_{d,c,h}$	pristine ice concentration production due to deposition nucleation, homogeneous freezing of cloud droplets, and homogeneous freezing of haze particles (m^{-3})
$(dN_t/dt)_{v,t,b}$	rate of pristine ice concentration production due to contact nucleation by diffusiophoresis, thermophoresis, and Brownian motion ($m^{-3}\ s^{-1}$)
p	atmospheric pressure (Pa)
p_{oo}	reference pressure = 10^5 Pa
P	general moment of gamma distribution (dimensionless)
Q	reference internal energy per unit mass of a category ($J\ kg^{-1}$)
$\dot{Q}$	source term for Q ($J\ kg^{-1}\ s^{-1}$)
Q_{lat}	energy per unit condensate mass required to evaporate and/or sublimate at constant temperature all condensate mass ($J\ kg^{-1}$)
Q^t, $Q^{t+\Delta t}$	values of Q at times t and $t+\Delta t$ ($J\ kg^{-1}$)
Q^*	temporary value of Q before heat and vapor diffusion ($J\ kg^{-1}$)
ΔQ_{vd}, ΔQ_{hd}	heating of category over a timestep due to vapor and heat diffusion ($J\ m^{-3}$)

r	mass mixing ratio of a category (kg kg^{-1})
r_{c+v}	the sum of r_c and r_v (kg kg^{-1})
r_{sl}, r_{si}	saturation mixing ratios over liquid and ice at air temperature T_a (kg kg^{-1})
r_v, r_c, r_r, r_p, r_s, r_a, r_g, r_h, r_t	mass mixing ratios of water vapor, cloud water, rain, pristine ice, snow, aggregates, graupel, hail, and the total over all forms of water (kg kg^{-1})
r_{vsh}	saturation mixing ratio at hydrometeor surface (kg kg^{-1})
r_{vs0}	reference value of saturation mixing ratio (kg kg^{-1})
r^*	temporary value of r before heat and vapor diffusion (kg kg^{-1})
Δr_i, Δr_l	mixing ratio contributions of ice and liquid water to coallescing hydrometeors (kg kg^{-1})
Δr_{ir}	mixing ratio of ice returned to ice category from coallesced hydrometeors (kg kg^{-1})
Δr_{it}	mixing ratio of ice transferred to new category following melting (kg kg^{-1})
Δr_{vd}	change of category mixing ratio over a timestep due to vapor diffusion (kg kg^{-1})
R, R_v	gas constants for dry air and water vapor (J kg^{-1} K^{-1})
S	hydrometeor shape parameter (dimensionless)
t, Δt	current time, model time increment (s)
T_a, T_{ac}	air temperature in (K) and (°C)
T_c	mean temperature of a category (°C)
T_{cc}	cloud droplet temperature (°C)
$T(P,x)$	the Pth moment of the incomplete gamma function (dimensionless)
T_0	reference temperature (°C)
v_t	terminal velocity of an individual hydrometeor (m s^{-1})
$\bar{v}_t$	mean value of v_t over a category size distribution (m s^{-1})
V_k	kinematic viscosity of air (m^2 s^{-1})
x, y	subscripts identifying colliding hydrometeor categories
z	absolute heights of top and bottom of a parcel of precipitation before and after falling for a timestep (m)
α_m	coefficient in mass power law formula (kg m$^{-\beta m}$)
α_{v_t}	coefficient in terminal velocity power law formula (ms^{-1} m$^{-\beta_{v_t}}$)
β_m	exponent in mass power law formula (dimensionless)
β_{v_t}	exponent in terminal velocity power law formula (dimensionless)
$\Gamma(\nu)$	complete gamma function of ν (dimensionless)
θ_{il}	ice–liquid potential temperature (K)
κ, κ_a	thermal conductivities of air and aerosol (J m^{-1} s^{-1})
λ	Marshall–Palmer slope parameter (m^{-1})
μ	dynamic viscosity of air (kg m^{-1} s^{-1})
ν	gamma distribution shape parameter (dimensionless)
ξ	quantity defined in Eq. (75) and used for autoconversion of cloud droplets to rain
π	3.14159
ρ_h, ρ_a	densities of a hydrometeor and dry air (kg m^{-3})
ρ_{va}	vapor density in atmosphere (kg m^{-3})
ρ_{vsh}	saturation vapor density at hydrometeor surface (kg m^{-3})
ρ_w	density of liquid water (kg m^{-3})
τ	quantity defined in Eq. (76) and used for autoconversion of cloud droplets to rain
ψ, ψ_a	vapor diffusivity and aerosol diffusivity in air (m^2 s^{-1})

nential or Marshall–Palmer distribution in which the modal diameter (the diameter where f_{gam} has a maximum value) is zero, while as ν increases, the modal diameter increases monotonically. The characteristic diameter D_n is used to nondimensionalize D, and serves as a diameter scaling factor for the distribution. It is related to the modal diameter by

$$D_{\text{mode}} = (\nu - 1)D_n \tag{3}$$

and to the mean diameter by

$$D_{\text{mean}} \equiv \int_0^\infty D f_{\text{gam}}(D)\,\mathrm{d}D = \frac{\Gamma(\nu+1)}{\Gamma(\nu)} D_n = \nu D_n. \tag{4}$$

In general, any moment P of the distribution is given by

$$\int_0^\infty D^P f_{\text{gam}}(D)\,\mathrm{d}D = D_n^P \frac{\Gamma(\nu+P)}{\Gamma(\nu)}. \tag{5}$$

The facility of Eq. (5) in providing an analytic solution to the integral is maintained for any property of the hydrometeor species which is expressed as a power of D. Two properties for which integrals are required are the mass m and the terminal velocity v_t. Expressing them as power law formulas

$$m = \alpha_m D^{\beta_m} \tag{6}$$

$$v_t = \alpha_{vt} D^{\beta_{vt}} \tag{7}$$

their concentration-normalized integrals become

$$\overline{m} = \alpha_m D_n^{\beta_m} \frac{\Gamma(\nu+\beta_m)}{\Gamma(\nu)}, \tag{8}$$

and

$$\overline{v}_t = \alpha_{vt} D_n^{\beta_{vt}} \frac{\Gamma(\nu+\beta_{vt})}{\Gamma(\nu)} \tag{9}$$

Fig. 1 is a plot of a family of gamma distributions, given by Eq. (1), where D_n is adjusted according to Eq. (8) such that all distributions have the same value of $\overline{m}$, and $\beta_m = 3$ is used. The abscissa is the hydrometeor diameter divided by the diameter $D_{\overline{m}}$ of the particle having mass $\overline{m}$. Integer values of ν from 1 to 10 are used. As ν increases, the distribution becomes progressively more peaked at $D = D_{\overline{m}}$.

Hydrometeor density is related to mass by

$$\rho_h \equiv \frac{\overline{m}}{Volume} = \frac{\alpha_m D^{\beta_m}}{\frac{\pi D^3}{6}} = \frac{6\alpha_m}{\pi} D^{\beta_m - 3}. \tag{10}$$

Multiplying Eq. (8) by N_t and dividing by air density ρ_a gives an expression for the mass mixing ratio of the hydrometeor category

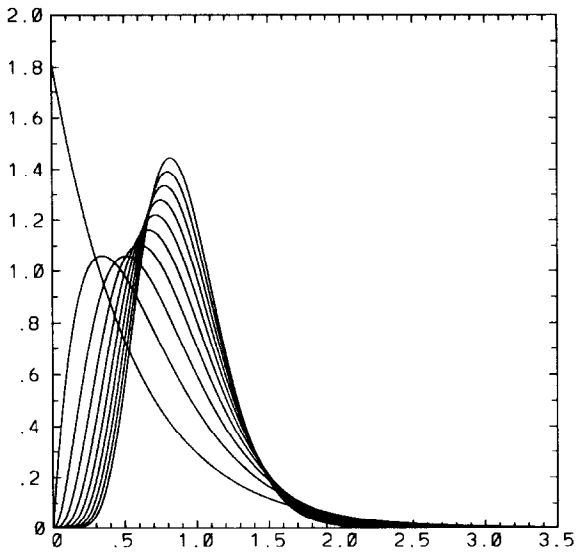

Fig. 1. Set of gamma distribution curves for integer values of the shape parameter ν from 1 to 10. The peaks of the curves shift progressively to the right as ν increases. Ordinate is the value of f_{gam} given by Eq. (1). Abscissa is hydrometeor diameter D, where $\overline{D_m}$ is held fixed at 1 for all curves, and β_m is set to 3.

$$r = \frac{N_t}{\rho_a} \alpha_m D_n^{\beta_m} \frac{\Gamma(\nu + \beta m)}{\Gamma(\nu)}. \tag{11}$$

In RAMS, the standard practice is to select the five parameters ν, α_m, β_m, α_{vt}, and β_{vt} for each category based on available empirical data, often with guidance from knowing the type of system being simulated, and to hold these parameters fixed in time and space for the duration of the simulation. (For the pristine ice and snow categories, multiple sets of these parameters are available, each describing a different crystal habit, and the option exists to switch during a simulation from one habit to another both spatially and temporally based on a pre-determined algorithm.) Once these parameters are specified, there remain two free parameters from the set (r, N_t, D_n) to be determined for each category, the third parameter being obtained from the other two and Eq. (11). The spatial and temporal dependence of the two free parameters are what define the model solution for each category. In the next section, we discuss the equations governing the two free parameters.

2.3. *Microphysical parameterization within the RAMS framework*

With the exception of cloud water and vapor, the mixing ratios of all water categories are governed by conservation equations of the form

$$\frac{\partial r}{\partial t} = \text{ADV}(r) + \text{TURB}(r) + \text{SOURCE}(r) + \text{SEDIM}(r) \tag{12}$$

where $r = [r_r, r_p, r_s, r_a, r_g, r_h, r_t]$ represents, respectively, the mixing ratios of rain, pristine ice, snow, aggregates, graupel and hail, plus an additional "total water" category consisting of the sum of the mixing ratios of all categories including cloud water and vapor (r_c and r_v). ADV (r) and TURB (r) represent advective and turbulent transport of r by the resolved and subgrid velocities in the model. SOURCE (r) represents source (and sink) terms for the categories which consist of all types of conversion of water substance from one category to another. SEDIM (r) represents local losses and gains of mixing ratio due to gravitational sedimentation. Eq. (12) is integrated forward in time from initial values (except for r_t, initial values are usually zero) to obtain prognostic mixing ratios for each model grid cell and each timestep.

The sum of the mixing ratios of cloud and vapor is determined as a difference of the prognostic mixing ratios:

$$r_{c+v} = r_t - (r_r + r_p + r_s + r_a + r_g + r_h). \tag{13}$$

The cloud mixing ratio r_c is then diagnosed as the amount, if any, by which the sum exceeds the saturation mixing ratio $r_{s\ell}$ with respect to liquid water:

$$r_c = \max[0, r_{c+v} - r_{s\ell}] \tag{14}$$

while r_v is diagnosed from

$$r_v = r_{c+v} - r_c. \tag{15}$$

Vapor mixing ratio r_v is thus not allowed to exceed $r_{s\ell}$}. Saturation mixing ratio $r_{s\ell}$ is given by

$$r_{s\ell} = \frac{0.622 e_{s\ell}}{p - e_{s\ell}} \tag{16}$$

where p is the atmospheric pressure and $e_{s\ell}$ is the saturation vapor pressure evaluated from an 8th order polynomial in air temperature T_a (Flatau et al., 1992). T_a is itself diagnosed from the prognostic ice–liquid potential temperature $\theta_{i\ell}$ and from the mixing ratios of all liquid and ice categories by the equation (Tripoli and Cotton, 1981)

$$T_a = \theta_{i\ell}\left(\frac{p}{p_{oo}}\right)^{R/C_p}\left[1 + \frac{Q_{lat}}{C_p \max(T_a, 253)}\right], \tag{17}$$

where Q_{lat} is given by

$$Q_{lat} = [r_r + r_c + (1 - i_g) r_g + (1 - i_h) r_h] L_{\ell v} + (r_p + r_s + r_a + i_g r_g + i_h r_h) L_{iv}, \tag{18}$$

and i_g and i_h are the fractional amounts of ice in the mixed-phase graupel and hail categories, respectively. Eqs. (14–18) and the equation for $e_{s\ell}$ are solved iteratively until convergence occurs. $\theta_{i\ell}$ is governed by an equation of the same form as Eq. (12), where SOURCE represents external heat sources such as radiative flux convergence, and SEDIM represents local sources or sinks due to sedimentation of ice or liquid water (Tripoli and Cotton, 1981). $\theta_{i\ell}$ is conservative in the absence of sedimentation and external heating.

Having provided either a prognostic or diagnostic means for determining all mixing ratio values r, one more distribution parameter (N_t or D_n) must be determined so that the other

may be diagnosed. RAMS has the options to (1) specify N_t, (2) specify D_n, (3) prognose N_t (though not for cloud water), or (4) in the special case where a category has a shape parameter ν of 1 [i.e., the Marshall–Palmer distribution (Kessler, 1969)], specify the value of N_0, where $N_t = N_0 D_n$, and $D_n = 1/\lambda$, where λ is the slope of the Marshall–Palmer distribution. When N_t is prognosed, it is governed by a conservation equation of the same form as Eq. (12) in which all terms are similar to those for mixing ratios. Except for testing purposes, N_t is always prognosed for pristine ice because it is the category into which nucleated ice is introduced, and the number of nucleated crystals is an important parameter to conserve. Other species, however, commonly use one of the other options above. The remainder of this section describes the SOURCE and SEDIM terms in Eq. (12) as applied to all prognostic mixing ratios and to the prognostic number concentration for pristine ice for the case where no other categories use a prognostic number concentration. Part II of this paper describes the SOURCE and SEDIM terms for number concentrations when they are prognosed in all categories.

2.4. *Vapor and heat diffusion and hydrometeor heat budget*

The temperature of a hydrometeor often differs substantially from that of the air due to latent heat release or absorption in the hydrometeor and sensible heating by collisions with other hydrometeors. The temperature, in turn, controls the rates of heat and vapor diffusion, and the amount of sensible heat transfer which occurs in coalescence of hydrometeors. In order to compute representative hydrometeor temperatures, we formulate a heat budget equation for each category. For convenience, we define a category reference energy in units of J kg^{-1}, relative to a reference state of ice at 0°C, by

$$Q = C_i T_c \text{ for ice}$$

$$Q = C_l T_c + L_{il} \text{ for liquid} \tag{19}$$

where T_c is the mean category temperature in °C, C_i and C_l are the specific heats of ice and liquid water, and L_{il} is the latent heat of fusion of water. Q is a more general variable than temperature in that it represents the energy associated not only with temperature but also with the latent heat of fusion. If Q is between zero and L_{il}, it implies that either the hydrometeor contains a mixture of ice and liquid at 0°C, with the liquid fraction given by Q/L_{il}, or that the hydrometeor is supercooled liquid. An energy equation for each ice and liquid category may be written in terms of Q as

$$\frac{dQ}{dt} = \dot{Q}_{vd} + \dot{Q}_{hd} + \dot{Q}_{conv} \tag{20}$$

where the three terms on the right represent sources or sinks associated with vapor diffusion, heat diffusion, and sensible heat transfer from mass conversion between categories. Melting or freezing of a hydrometeor do not constitute an external heat source or sink of Q, although they can affect the hydrometeor temperature and therefore any of the source terms.

The definition of Q in Eq. (19) provides a convenient means for evaluating the third source term in Eq. (20). Whenever an amount of mixing ratio r_1 with energy Q_1 is converted from one ice or liquid category to another, either by coalescence or by recategorization as

when an ice particle melts into rain, it carries with it the energy product $Q_1 r_1$. Both r_1 and $Q_1 r_1$ are subtracted from the old category and added to the new. Given a category mixing ratio and energy r^t and Q^t at a given time t, new values r^* and Q^* are computed following all such transfers in the timestep by the equations

$$r^* = r^t + \Sigma_{r_1} \tag{21}$$

and

$$Q^* = (Q^t r^t + \Sigma Q_1 r_1)/r^*. \tag{22}$$

Multiplying Eq. (20) by Δt and substituting Eq. (22) gives an expression for Q on the next timestep $t + \Delta t$

$$Q^{t+\Delta t} = (\dot{Q}_{\mathrm{vd}} + \dot{Q}_{\mathrm{hd}})\Delta t + Q^*. \tag{23}$$

The net difference $Q^{t+\Delta t} - Q^t$ over a timestep constitutes a heat storage term for the category which is most significant relative to other terms in Eq. (22) and Eq. (23) when the value of D_n is largest.

It is not practical to solve Eq. (23) explicitly because the heat and vapor diffusion terms are very sensitive to temperature and would necessitate the use of a very small time step for stable integration. A second consequence of their sensitivity is that they are the strongest regulators of hydrometeor temperatures compared with the conversion term. A practical means for obtaining a stable category temperature is thus to solve the diffusion and time dependent terms implicitly by expressing them as a function of temperature at time $t + \Delta t$. To develop this equation, we begin with the vapor diffusion equation for a single hydrometeor (Pruppacher and Klett, 1978)

$$\frac{\mathrm{d}m}{\mathrm{d}t} = 2\pi D \psi f_{Re}(\rho_{\mathrm{va}} - \rho_{\mathrm{vsh}}). \tag{24}$$

where ψ is the vapor diffusivity. The ventilation coefficient f_{Re} is given by (Cotton et al., 1982)

$$f_{Re} = \left[1.0 + 0.229\left(\frac{v_t D}{V_k}\right)^{0.5}\right] S, \tag{25}$$

where S is the shape parameter and V_k is the kinematic viscosity of air.

Multiplying by the distribution function (Eq. 2) and integrating over the distribution gives the mass diffusion rate per cubic meter of atmosphere:

$$N_t \frac{\mathrm{d}\bar{m}}{\mathrm{d}t} = N_t 2\pi\psi F_{Re}(\rho_{\mathrm{va}} - \rho_{\mathrm{vsh}}) \tag{26}$$

where

$$F_{Re} \equiv \int_0^\infty D f_{Re} f_{\mathrm{gam}}(D)\,\mathrm{d}D \tag{27}$$

is the integrated product of ventilation coefficient and diameter. Here, we have tacitly assumed that ρ_{vsh}, and therefore hydrometeor temperature, is independent of diameter. Dividing Eq. (26) by ρ_a and multiplying by Δt gives the change in category mixing ratio in a timestep due to vapor diffusion

$$\Delta r_{vd} = N_t 2\pi\psi F_{Re} \Delta t (r_v - r_{vsh}). \tag{28}$$

Because we are now dealing with a finite time interval, we must account for adjustments to atmospheric vapor r_v during the timestep due to the vapor transfer described by Eq. (28). In keeping with the goal of deriving an implicit equation, we replace r_v by $r_v - \Delta r_{vd}$ in Eq. (28) to represent the vapor remaining at the end of the time interval Δt. Solving for Δr_{vd} gives

$$\Delta r_{vd} = \frac{N_t 2\pi\psi F_{Re} \Delta t (r_v - r_{vsh})}{1 + N_t 2\pi\psi F_{Re} \Delta t}, \tag{29}$$

in which the denominator is greater than 1 and thus reduces Δr_{vd} compared to Eq. (28). Eq. (29) prevents over-depletion of ambient vapor by diffusion to hydrometeors for any length timestep. Multiplying Eq. (29) by latent heat L (L_{lv} or L_{iv} depending on the category) and by ρ_a gives the latent heating of the category over a timestep by vapor diffusion,

$$\Delta Q_{vd} = BL\rho_a N_t 2\pi\psi F_{Re} \Delta t (r_v - r_{vsh}), \tag{30}$$

where

$$B = \frac{1}{1 + N_t 2\pi\psi F_{Re} \Delta t}. \tag{31}$$

The sensible heat diffused to a category is, in analogy to Eq. (28),

$$\Delta Q_{hd} = N_t 2\pi\kappa F_{Re} \Delta t (T_{ac} - T_c), \tag{32}$$

where κ is the thermal conductivity of air. We add Eq. (30) and (32), and then divide by $(\rho_a r)$ to get the category heating over a timestep in J kg^{-1} due to latent plus sensible heat diffusion. Substituting this expression for the diffusion terms in Eq. (23) gives

$$Q^{t+\Delta t} = C[BL\rho_a \psi (r_v - r_{vsh}) + \kappa (T_{ac} - T_c)] + Q^*, \tag{33}$$

where

$$C = \frac{2\pi F_{Re} N_t \Delta t}{\rho_a r}. \tag{34}$$

To close Eq. (33), we write a linearized form of the Clausius–Clapeyron equation combined with Eq. (16):

$$r_{vsh} = r_{vs0} + \left(\frac{dr_{vsh}}{dT}\right)_0 (T_c - T_0), \tag{35}$$

where the subscript 0 signifies a reference value. We note here the work reported in Srivastava and Coen (1992) which showed that a quadratic form of this equation leads to a significantly better approximation. They used the ambient atmospheric temperature as the

reference value such that in cases where the hydrometeor temperature differs substantially from the atmospheric value, the linear approximation given in Eq. (35) indeed gives poor accuracy. By experimentation, we have found that if a reference temperature is chosen using the formula

$$T_0 = T_{ac} - \min[25{,}700(r_{s\ell} - r_v)], \tag{36}$$

for application to liquid hydrometeors, and

$$T_0 = \min(0, T_0), \tag{37}$$

for ice hydrometeors, the linear approximation is very good over all ranges of conditions found in the atmosphere, and avoids the added complication of a quadratic approximation. Substitution of Eq. (35) into Eq. (33) gives

$$Q^{t+\Delta t} = C\left\{BL\rho_a\psi\left[r_v - r_{vs0} - \left(\frac{dr_{vsh}}{dT}\right)_0 (T_c - T_0)\right] + \kappa(T_{ac} - T_c)\right\} + Q^* \tag{38}$$

in which all terms are known beforehand, except $Q_{t+\Delta t}$ and T_c which must be solved with the help of Eq. (38) and the implicit relation that T_c is defined at time $t+\Delta t$. Eq. (38) along with Eq. (22) is the general equation used to compute the energy Q and temperature T_c for all categories, but is subject to different constraints and conditions for each category.

For rain not contacting ice particles we assume that supercooling rather than freezing occurs with temperatures below 0°C. Thus we always have

$$T_c = \frac{Q_{t+\Delta t} - L_{il}}{C_l}, \tag{39}$$

so Eq. (38) becomes

$$Q^{t+1} = L_{il} + \frac{C\left\{BL_{lv}\rho_a\psi\left[r_v - r_{vs0} + \left(\frac{dr_{vsh}}{dT}\right)_0 T_0\right] + \kappa T_{ac}\right\} + (Q^* - L_{il})}{1 + C\left[BL_{lv}\rho_a\psi\left(\frac{dr_{vsh}}{dT}\right)_0 + \kappa\right]/C_l}. \tag{40}$$

For pristine ice, snow and aggregates, a number of simplifications can be made to Eq. (38). The heat storage term $(Q^{t+\Delta t} - Q^t)$ implicit in the equation is neglected under the reasoning that these hydrometeors have such a low mass-to-surface-area ratio that the diffusion terms will dominate. The conversion term in Eq. (20) is neglected because, as will be described later, conversions involving pristine ice, snow, or aggregates with cloud water, rain, graupel, and/or hail always result in mass and energy being removed, not added. In such conversions, the mean energy Q of the remaining pristine ice, snow, or aggregates is unaffected. There are also conversions between pristine ice and snow, and from pristine ice and/or snow to aggregates. They also produce no changes in Q, however, because the remaining terms in (Eq. 38) (sensible and latent heat diffusion) are identical for these categories and thus tend to produce the same value of T_c for all. Thus, Eq. (38) reduces to

$$T_c = \frac{BL_{iv}\rho_a\psi\left[r_v - r_{vs0} + \left(\frac{dr_{vsh}}{dT}\right)_0 T_0\right] + \kappa T_{ac}}{BL_{iv}\rho_a\psi\left(\frac{dr_{vsh}}{dT}\right)_0 + \kappa} \tag{41}$$

which is a commonly used equation for hydrometeor temperature derived from an assumed balance between sensible heat diffusion and latent heat release from vapor diffusion. However, T_c must be constrained to remain at or below zero for these ice categories. If the solution to Eq. (41) is above zero, it implies that melting must occur. Physically, the latent heat absorbed by melting holds T_c at zero, causing a net diffusive influx of latent plus sensible heat which determines the melting rate. In this case, Eq. (41) is replaced with a version of Eq. (33) in which T_c and Q^* are set to zero, and r_{vsh} is the value at 0°C

$$Q^{t+\Delta t} = C[BL_{\ell v}\rho_a\psi(r_v - r_{vsh}(0)) + \kappa T_{ac}]. \tag{42}$$

The resulting value of $Q^{t+\Delta t}$ is positive, and its magnitude divided by L_{il} gives the fractional amount (not to exceed 1) of ice melted in the category due to diffusion during the given timestep. Melting of these ice categories implies conversion to graupel or rain, a decision process which is discussed in the next two sections.

For graupel and hail, both the heat storage and conversion terms in Eq. (38) and Eq. (20) are retained as for rain. Since these categories allow both ice and liquid phases to be present, Q and Q^* may be of either sign, and may or may not be of the same sign. The relation between T_c and $Q^{t+\Delta t}$ depends on these signs. If Q^* is negative, implying the category is totally ice, we first try setting $T_c = Q^{t+\Delta t}/C_i$ to obtain

$$Q^{t+\Delta t} = \frac{C\left\{BL_{iv}\rho_a\psi\left[r_v - r_{vs0} + \left(\frac{dr_{vsh}}{dT}\right)_0 T_o\right] + \kappa T_{ac}\right\} + Q^*}{1 + C\left[BL_{iv}\rho_a\psi\left(\frac{dr_{vsh}}{dT}\right)_0 + \kappa\right]/C_i}. \tag{43}$$

If a negative or zero value of $Q^{t+\Delta t}$ results, it implies that no latent heat absorption due to melting occurs and Eq. (43) is valid. If $Q^{t+\Delta t}$ turns out positive, we return to Eq. (33) as for pristine ice, snow, and aggregates, and set T_c to zero and r_{vsh} to the value at 0°C. The term Q^* is retained for graupel and hail. This gives the same result as Eq. (42) except that the source term Q^* is added to the right hand side.

If Q^* is positive for graupel or hail, the category is of mixed phase and T_c is zero. Thus, we again apply Eq. (42) with Q^* on the right hand side. If this results in a positive or zero value of $Q^{t+\Delta t}$, it is concluded that T_c remained positive throughout the timestep and that the result is valid. If, however, a negative value of $Q^{t+\Delta t}$ results, it is concluded that sensible and latent heat diffusion first froze all liquid in the category, and then lowered its temperature below zero. The amount of time left in the timestep after freezing occurs is computed from

$$\Delta t_R = \Delta t\left(\frac{Q^{t+\Delta t}}{Q^{t+\Delta t} - Q^*}\right). \tag{44}$$

A final (negative) value of $Q^{t+\Delta t}$ is then evaluated from Eq. (43) in which Q^* is set to zero and Δt_R replaces Δt in Eq. (34). As for pristine ice, snow, and aggregates, the value of $Q^{t+\Delta t}$ evaluated here gives not only temperature, but also the fraction of liquid present. For graupel and hail, however, conversion may or may not result from melting. The decisions behind the conversion process are discussed in the next two subsections. The advantage of allowing mixed-phase hydrometeor categories is that it allows more accurate prediction of radar reflectivity and also the amounts of water mass shed from hailstones.

The hydrometeor temperatures (or Q values) derived in this section implicitly include the effect of vapor diffusion, and are consequently the temperatures which govern the vapor diffusion rates. Thus, the amount of vapor diffused to a category in a timestep is evaluated directly from Eq. (29), in which r_{vsh} is evaluated from Eq. (35).

A sink for the number concentration N_t of pristine ice results when the vapor diffusion to pristine ice is negative (i.e., when sublimation occurs). A parameterization for this sink is described in Harrington et al. (1995), and is formulated in terms of a function F_e appearing in the equation

$$\frac{\Delta N_t}{N_t} = F_e\left(\frac{\Delta r}{r}, \nu, H\right). \tag{45}$$

The left hand side of Eq. (45) is the fractional number lost in a timestep, and F_e is a function of three variables: the fractional mixing ratio lost in the timestep, the gamma function shape parameter ν and the habit H of pristine ice. Harrington evaluates F_e for specific values of ν and H, and for fine increments of the quotient $\Delta r/r$ between 0 and 1 using an explicit ice evaporation model with numerous size bins. In RAMS, F_e is implemented as a lookup table.

2.5. *Collision and coalescence of hydrometeors*

Differential fall speeds between individual hydrometeors of the same or different categories cause some of them to collide and coalesce. Depending on the categories, masses and temperatures (or Q values) of the two colliding hydrometeors, a decision is made as to where to transfer the mass of coalesced hydrometeor. The rate at which the mixing ratio r_x of species x is collected into coalesced hydrometeors due to collisions with hydrometeors of species y is given by the stochastic collection equation (Verlinde et al., 1990)

$$\frac{\mathrm{d}r_x}{\mathrm{d}t} = \frac{N_{tx} N_{ty} \pi F_\rho}{4\rho_a} \int_0^\infty \int_0^\infty m(D_x)\,(D_x + D_y)^2 \,|v_{tx}(D_x) - v_{ty}(D_y)|\, f_{\mathrm{gam}x}(D_x) f_{\mathrm{gam}y}(D_y) E(x,y)\,\mathrm{d}D_x \mathrm{d}D_y \tag{46}$$

where f_{gam}, m, and v_t are defined in Eqs. (1), (6) and (7), respectively. The collection efficiency $E(x, y)$ is the product of collision efficiency and coalescence efficiency. The additional factor F_ρ not appearing in Verlinde et al. is equal to $(1/\rho_a)^{0.5}$ and accounts for the density effect on the terminal fall velocities.

Verlinde et al. (1990) assumed that $E(x, y)$ is independent of D_x and D_y so that it can be moved outside the integrals, a reasonable assumption for all hydrometeor classes but cloud droplets, where E varies strongly over the cloud droplet spectrum. They found analytic

Table 2
Categories

Collected category	Collecting category	Destination category
cloud water	rain	rain
pristine ice	pristine ice	aggregates
pristine ice	snow	aggregates
snow	pristine ice	aggregates
pristine ice	aggregates	aggregates
pristine ice	graupel	graupel
pristine ice	hail	hail
snow	snow	aggregates
snow	aggregates	aggregates
snow	graupel	graupel
snow	hail	hail
aggregates	graupel	graupel
aggregates	hail	hail
graupel	hail	hail

solutions to Eq. (46) in terms of known functions, but found it more computationally expedient to solve only the integral over D_y analytically while numerically computing the integral over D_x (J. Verlinde, pers. commun.). That procedure is followed here. To further reduce the computational effort during model runtime, a large number of solutions to the integral are pre-computed and tabulated in a three-dimensional look-up table. Two of the table dimensions are the characteristic diameters D_{nx} and D_{ny} which occur in $f_{\mathrm{gam}x}$ and $f_{\mathrm{gam}y}$. The third dimension is the pair (x, y) of interacting categories ranging over 32 of the 49 total possible pairs that can be formed from the seven liquid and ice categories. The number of table entries required for a given level of accuracy is minimized by spacing the entries in uniform increments of $\log(D_{nx})$ and $\log(D_{ny})$, and 60 entries spanning a four orders-of-magnitude range of each of the characteristic diameters has been found to be adequate. Thus, the table contains $32 \times 60 \times 60$ entries.

During model runtime, for any given pair (x, y), values are interpolated from the table bi-linearly over $\log(D_{nx})$ and $\log(D_{ny})$ to efficiently obtain a value for the double integral in Eq. (46). Multiplying the equation by Δt gives the amount of r_x coalescing with category y over a timestep

$$\Delta r_x = \frac{N_{tx} N_{ty} \pi F_\rho E(x,y)\, \Delta t}{4\rho_a} J[(x,y), D_{nx}, D_{ny}] \tag{47}$$

where J is the interpolated table value. In some cases, unless Δt is small enough, Eq. (47) gives a value of Δr_x which is greater than r_x. For example, mixing ratio rates of hail particles colliding with cloud droplets and cloud droplets colliding with hail particles are both computed, as described below. Since all hail particles inside a cloud will undergo collision with a cloud droplet almost instantaneously, the hail collection rate is extremely large. Thus, Δr_x is limited to a maximum value of r_x.

Hydrometeor collections are divided into two classes, each with its own basic rules for determining the destination category or categories to which Δr_x is transferred. The first class only treats collisions between liquid and liquid or between ice and ice (mixed phase

categories considered as ice here). The destination is a single category, pre-determined as a function of the interacting pair (x, y) only and independent of the energies Q_x and Q_y. Table 2 lists the collected, collecting, and destination categories for all collections in this class. Note that in cases where the destination category is different from both the collected and collecting categories, the collection is repeated with the collected and collecting categories reversed. This is how mixing ratio is extracted from both colliding categories for transfer to the destination category. Also, when the colliding categories are identical, the collected amount is simply doubled to avoid the need for duplicating the computation with the colliding categories reversed. As mentioned in the previous section, a quantity of energy $Q_x \Delta r_x$ accompanies the mixing ratio Δr_x from the collected to the destination category.

The second class of collections treats mixed-phase collisions between cloud water or rain and any of the ice categories (except that cloud water and pristine ice interactions are neglected). For each of these collisions, two collection amounts are computed by Eq. (47): the ice Δr_i collected by liquid, and the liquid Δr_l collected by ice. Except for cloud water which is diagnostic, these mixing ratios along with the corresponding energy values $Q_i \Delta r_i$ and $Q_r \Delta r_l$ are subtracted from the collected categories. The total mixing ratio of the coalesced hydrometeors is

$$r^* = \Delta r_i + \Delta r_l \tag{48}$$

and their energy value is evaluated from

$$Q^* = (Q_i \Delta r_i + Q_r \Delta r_l)/r^* \tag{49}$$

similar to Eq. (22). The fractional amount of liquid contained in the coalesced hydrometeors after the two contributors reach thermal equilibrium with each other is the quotient Q^*/L_{il}, limited to the range (0, 1). If this fraction is 1, r^* is transferred to the rain category along with energy $Q^* r^*$. Otherwise, r^* and $Q^* r^*$ are divided between the input ice category and a secondary ice category, which is graupel in the case where Δr_l represents cloud water, and hail where it represents rain. If ice contributed most of the mass to the coalesced hydrometeors and if they remain mostly ice because little or no melting takes place, then the coalesced hydrometeors are assumed to retain much of the characteristic structure of the input ice, and most of r^* and $Q^* r^*$ are returned to the input ice category. With somewhat greater relative inputs from the liquid category, and/or with significant melting of the coalesced hydrometeors, most or all of r^* and $Q^* r^*$ is transferred to graupel or hail. We are currently testing the formula

$$\Delta r_{ir} = \Delta r_i \frac{Q^*}{L_{il}} \tag{50}$$

to determine the amount of ice returned to the input ice category; the remainder is transferred to the secondary ice category. If graupel is the input ice category, the secondary category is hail, even if cloud water is the liquid being collected. If hail is the input ice category, the only output ice category is hail. This formulation is partly based on the reasoning that coalesced hydrometeors will vary in their ratios of collected ice versus collected liquid because of the size ranges within both input categories, and will thus vary in the category they best fit into.

When the number concentration N_t is prognosed for pristine ice only, it is decreased in the same proportion as mixing ratio each timestep when collection results in conversion of pristine ice to other categories. Part II will describe a scheme for evaluating the number sink when N_t is prognosed for all categories.

2.6. Ice nucleation

Nucleation of pristine ice crystals may occur by a variety of physical mechanisms. These may be divided into two general categories: heterogeneous nucleation, in which an ice nucleus (IN) is responsible for initializing an ice crystal structure from vapor or liquid, and homogeneous nucleation where an IN is not involved. Parameterizations representing both heterogeneous and homogeneous nucleation are described here.

Deposition nucleation is a form of heterogeneous nucleation in which vapor molecules attach to an IN, and may occur any time the ambient vapor mixing ratio exceeds saturation over ice, and the temperature is below -5°C. Condensation-freezing nucleation occurs when an aerosol has the properties of both a cloud condensation nucleus (CCN) and an IN. Vapor molecules attach as liquid to the aerosol for its CCN property, and then freeze from its IN property. Condensation-freezing nucleation requires supersaturation with respect to liquid water, and temperatures below -2°C. Both these types of nucleation are represented by a single empirically-based parameterization described by Meyers et al. (1992). This parameterization is a function of the supersaturation with respect to ice r_{si}, and is given by

$$(N_t)_d = \exp(6.269 + 12.96 r_{si}) \tag{51}$$

where $(N_t)_d$ is the number of nucleated crystals per m^3. The number $(N_t)_d$ is given as a total number of crystals which can nucleate under the given environmental conditions, and is not dependent on time or on the length of the model timestep. In RAMS, when pristine crystals are prognosed and already exist locally on a given timestep, the condensation-freezing process produces fewer crystals so that the total number will equal $(N_t)_d$. When the existing number of crystals exceeds this amount, they are allowed to remain, but no additional condensation-freezing nucleation is performed.

Contact freezing nucleation occurs when an IN comes into contact with an existing supercooled cloud water droplet. Transport of the IN to the droplet results from a combination of diffusiophoresis, thermophoresis and Brownian motion. Diffusiophoresis occurs in supersaturated environments where droplets are growing by condensation, and is a process in which the net vapor mass flux toward the droplet carries IN in the flow. In RAMS, since exact saturation is assumed when diagnosing an amount of cloud water, a separate estimate of supersaturation is obtained by applying Eq. (29) to cloud water, computing Δr_{vd} as a residual of the net change in cloud water mixing ratio over a timestep minus all source terms (such as collection) other than vapor deposition, and taking r_v in the equation as the ambient supersaturation. Thermophoresis occurs in subsaturated environments when cloud droplets exist but are evaporating. It is a flux of aerosols toward the droplet resulting from the gradient of air molecular speed (temperature) when the droplet is evaporatively cooled below the environmental temperature. As for diffusiophoresis, the separate estimate of subsaturation is used. Thermophoresis dominates over diffusiophoresis, so their net effect is to increase contact nucleation in subsaturated conditions and decrease it in supersaturated

conditions. Brownian motion is a random-walk transport of aerosols due to collisions with air molecules, and results in some IN colliding with cloud droplets.

Parameterizations of the numbers of crystals produced by contact nucleation due to diffusiophoresis, thermophoresis and Brownian motion are described in Cotton et al. (1986) and are given by, respectively,

$$\left(\frac{dN_t}{dt}\right)_v = F_1 F_2 \frac{R_v T_a}{L_{lv}\rho_a} \tag{52}$$

$$\left(\frac{dN_t}{d_t}\right)_t = \frac{F_1 F_2 f_t}{\rho_a}, \tag{53}$$

and

$$\left(\frac{dN_t}{dt}\right)_b = F_1 \psi_a, \tag{54}$$

where ψ_a is the aerosol diffusivity. The expressions F_1, F_2 and f_t are defined by

$$F_1 = 2\pi D_c N_{tc} N_a, \tag{55}$$

$$F_2 = \frac{\kappa}{p}(T_{ac} - T_{cc}), \tag{56}$$

and

$$f_t = \frac{0.4[1 + 1.45K_n + 0.4K_n \exp(-1/K_n)](\kappa + 2.5K_n\kappa_a)}{(1+3K_n)(2\kappa + 5\kappa_a K_n + \kappa_a)}, \tag{57}$$

where D_c is the cloud droplet diameter, N_{tc} is the cloud droplet concentration, N_a is the concentration of active contact nuclei, κ_a is the aerosol thermal conductivity, K_n is the Knudsen number, and T_{cc} is the cloud droplet temperature. The Knudsen number K_n is defined as

$$K_n = \frac{\lambda_{a0} T p_0}{T_0 p R_a}, \tag{58}$$

where $\lambda_{a0} = 6.6 \times 10^{-8}$ m is the mean free path at reference temperature $T_0 = 293.15$ K and reference pressure $p_0 = 101325$ Pa, and R_a is the aerosol radius. The aerosol diffusivity ψ_a is defined by

$$\psi_a = \frac{kT_{cc}}{6\pi R_a \mu}(1 + K_n), \tag{59}$$

where k is the Boltzmann constant, and μ is the dynamic viscosity of air. A parameterization for the number of IN per m^3 available for contact freezing nucleation is described in Meyers et al. (1992), and is given by

$$N_a = \exp(4.11 - 0.262T_{cc}), \tag{60}$$

where a contact nuclei size of 10^{-7} m is assumed.

Homogeneous nucleation of supercooled water is a spontaneous process in which a small group of water molecules take on a crystal lattice structure due to random motions. Once the structure is begun, it quickly grows throughout the entire water droplet. The probability of a given number of molecules initiating an ice lattice in a unit time interval is a function primarily of temperature, but also depends on the amount and type of impurities of the water, and on the droplet curvature. The probability of a given droplet having an ice nucleus form anywhere within it (resulting in freezing of the entire droplet) is, in addition to the above, a strong function of the droplet volume. For activated cloud droplets where the solute and curvature effects are negligible, DeMott et al. (1994) derived from empirical data the following expression to represent the number of cloud droplets freezing in a timestep

$$(N_t)_c = N_t \int_0^\infty \left[1 - \exp\left(-10^{\phi} \frac{\pi D^3}{6} \Delta t \right) n(D) \right] \mathrm{d}D \tag{61}$$

where

$$\phi = -606.3952 - 52.6611 T_{cc} - 1.7439 T_{cc}^2 - 0.0265 T_{cc}^3 - 0.0001536 T_{cc}^4. \tag{62}$$

This nucleation formula is applied in the temperature range $-50°C < T_{cc} < -30°C$. At colder temperatures, the value at $-50°C$ is applied, which is essentially nucleation of all cloud droplets. For a given Δt and cloud distribution shape parameter, both of which are constant in time in RAMS, the integral in Eq. (61) is a function of T_{cc} and D_n only. For computational efficiency, the integral is pre-computed for many values of T_{cc} and D_n to create a two-dimensional table of values, and required values are bi-linearly interpolated from the table during model execution.

For unactivated haze particles, DeMott et al. (1994) derived the equation

$$f_{\mathrm{nuc}} = \int_0^{D_{\max}} \exp\left(-\frac{D}{D_n} \right) \left[1 - \exp\left(\frac{D}{D_e} \right)^b \right] \frac{\mathrm{d}D}{D_n}, \tag{63}$$

which describes the fractional number of haze particles freezing homogeneously in a unit time of one second. Here, D and D_n refer to the CCN spectrum, which we have generalized to follow a gamma distribution as in Eq. (2). The quantities D_e and b are complicated functions of atmospheric temperature and relative humidity, and the type of solute, assumed to be ammonium sulfate in this work, and $D_{\max} = 1.02 \times 10^{-6}$ m (DeMott et al., 1994). Assuming a fixed background CCN spectrum, the integral in Eq. (63) is thus a function of only temperature and relative humidity. As is done for evaluating the number of nucleating cloud droplets, the integral values are pre-computed and stored in a two-dimensional table, from which required values are later interpolated. The fraction of haze particles freezing in a model timestep Δt is approximated by the bracketed term in the following equation, and is of a form which cannot exceed 1. The actual number freezing is given by

$$(N_t)_h = N_h [1 - \exp(-f_{\mathrm{nuc}} \Delta t)], \tag{64}$$

where N_h is the number concentration of haze particles. The total number of nucleating ice crystals by all processes is given by

$$\Delta N_t = (N_t)_d + (N_t)_c + (N_t)_h + \left[\left(\frac{dN_t}{dt}\right)_v + \left(\frac{dN_t}{dt}\right)_t + \left(\frac{dN_t}{dt}\right)_b\right]\Delta t, \tag{65}$$

which is added to the number concentration N_t for pristine ice. The nucleation contribution to mixing ratio is evaluated from the expression

$$\Delta r_p = \Delta N_t m_n / \rho_a \tag{66}$$

where m_n is an assumed initial mass of a nucleated particle.

2.7. *Other conversions*

Thus far we have discussed the conversion of mass from one category to another that results from nucleation of pristine ice from a vapor or cloud water source, diffusive flux of vapor to and from liquid and ice, and collisions between hydrometeors (including the effect of melting or freezing upon collision). Additional conversions which are parameterized in the model are discussed in this section.

Secondary ice production based on the Hallett–Mossop theory is parameterized as reported in Cotton et al. (1986). This is a process connected with riming in which a fraction of the rime splinters into tiny crystals. A transfer of mixing ratio to pristine ice from the other ice categories is carried out when riming occurs, and the number of pristine crystals is increased. A transfer of mixing ratio from pristine ice to snow is carried out when pristine ice grows by vapor deposition, and a reverse transfer is made when snow evaporates (Harrington, 1994). This is in keeping with our definition of the snow category as containing "mostly pristine" ice crystals of larger diameter than those in the pristine ice category. The transfer to snow during vapor deposition is assumed to be made on the larger crystals in the pristine ice distribution, while the reverse transfer during evaporation is assumed to be on the smaller snow crystals. This keeps the characteristic diameters of both categories within their assumed ranges. A constant threshold diameter D_b, which we currently set to 1.25×10^{-4} m, is used as an upper bound to the pristine ice characteristic diameter and a lower bound to the snow characteristic diameter. This value is based on ice crystal size-spectra observed in cirrus clouds (Arnott et al., 1993; Mitchell et al., 1993). While both pristine ice and snow follow complete gamma distributions and therefore implicitly contain crystals of all diameters, the part of either distribution contained on the far side of D_b (the largest pristine ice or the smallest snow) is what is assumed to be involved in the conversion.

The mass and number transfer rates of pristine ice to snow are taken as the rates of mass and number growth of the pristine ice distribution in the region $D_b < D < \infty$ due to vapor deposition. These may be expressed as

$$\left(\frac{dr}{dt}\right)_{p\to s} = \frac{d}{dt}\left[\frac{1}{\rho_a}\int_{D_b}^{\infty} \alpha_m D^{\beta m} n(D)\,dD\right]_{vp} \tag{67}$$

$$\left(\frac{dN_t}{dt}\right)_{p\to s} = \frac{d}{dt}\left[\int_{D_b}^{\infty} n(D)\,dD\right]_{vp} \tag{68}$$

where the subscripts v and p refer to the vapor deposition process and the pristine ice category. By applying Leibniz' rule, chain differentiating, and using Eq. 26 the following forms of the above equations are obtained

$$\left(\frac{\mathrm{d}r}{\mathrm{d}t}\right)_{p\to s} = \left[\frac{\Gamma(\nu)}{D_n\Gamma(\nu+1)}\left(\frac{D_b^2 n(D_b)}{\beta_m} + T(1, D_b/D_n)\right)\right]_p \left(\frac{\mathrm{d}r}{\mathrm{d}t}\right)_{\mathrm{vp}}, \tag{69}$$

$$\left(\frac{\mathrm{d}N_t}{\mathrm{d}t}\right)_{p\to s} = \left[\frac{\Gamma(\nu)\rho_a D_b^{2-\beta_m} n(D_b)}{D_n\Gamma(\nu+1)\alpha_m\beta_m I(1)}\right]_p \left(\frac{\mathrm{d}r}{\mathrm{d}t}\right)_{\mathrm{vp}}, \tag{70}$$

where $T(1,D_b/D_n)$ is the first moment of the incomplete gamma distribution described in general as,

$$T(P,X) = \int_X^\infty D^P n(D)\,\mathrm{d}D = \frac{N_t D_n^P}{\Gamma(\nu)} I\left(\nu+\beta, \frac{X}{D_n}\right). \tag{71}$$

Eq. (70) describes the rate of change in number concentration in the region $D_b < D < \infty$ due to the spectral shift of pristine ice crystals across the diameter threshold D_b. The first term in Eq. (69) is analogous, but applies to the mass contained in the crystals that cross D_b. The second term describes the vapor depositional growth of pristine ice mass in the region $D_b < D < \infty$. This second term is kept in the description of mass transfer because it is a mass source for snow.

The corresponding equations for mass and number transfer from snow to pristine ice when snow evaporates are

$$\left(\frac{\mathrm{d}r}{\mathrm{d}t}\right)_{\mathrm{s}\to\mathrm{p}} = \left[-\frac{\Gamma(\nu)D_b^2 n(D_b)}{D_n\Gamma(\nu+1)\beta_m}\right]_s \left(\frac{\mathrm{d}r}{\mathrm{d}t}\right)_{\mathrm{vs}} \tag{72}$$

$$\left(\frac{\mathrm{d}N_t}{\mathrm{d}t}\right)_{\mathrm{s}\to\mathrm{p}} = \left[\frac{\Gamma(\nu)\rho_a D_b^{2-\beta_m} n(D_b)}{D_n\Gamma(\nu+1)\alpha_m\beta_m}\right]_s \left(\frac{\mathrm{d}r}{\mathrm{d}t}\right)_{\mathrm{vs}}, \tag{73}$$

where the subscript s refers to the snow category. Eq. (69) is analogous to Eq. (72), except that the second term, which represents a source for snow in Eq. (69), is dropped, because physically it represents evaporation and is thus not a source for the pristine ice category. When N_t is prognosed only for pristine ice, the only available N_t value for snow is that which is specified or diagnosed. That value, however, can be used to estimate the number concentration $n(D_b)$ at the cutoff diameter from Eq. (2).

During ambient conditions that are subsaturated with respect to ice, there exists the possibility of number concentration "build-up" in the pristine ice category. In order to correct this, a scheme in which pristine ice number concentration loss to evaporative processes has been developed. This was accomplished by noting that the fractional number loss ratio $\Delta N_t/N_t$, should be a strong function of the pristine ice fractional mass loss ratio $\Delta r_p/r_p$, and of the distribution shape parameter, ν. Using this hypothesis a bin model was constructed in which the number loss ratio was found as a function of the mass loss ratio and the shape parameter, ν. Look-up tables were constructed for the number loss ratio for ranges of mass loss from 0.01 to 1.0, ν values from 1 to 5 and over all of the different crystal habits. Testing of the model shows that variation in external parameters (such as

temperature, pressure, saturation, and D_n) affect the number loss ratio only to a small degree. Values of D_n can cause the most variation, however this occurs only over very wide ranges of D_n.

Collision and coalescence of cloud droplets to form rain is not readily treated by solving the stochastic collection equation due to the large gap in diameters of cloud droplets and rain, and to the strong variations of $E(x, y)$ with cloud droplet diameter. Thus, we use a separate autoconversion parameterization (Berry and Reinhardt, 1974) given by

$$\frac{\mathrm{d}r_r}{\mathrm{d}t} = \frac{\rho_w \xi}{\rho_a \tau}, \tag{74}$$

where

$$\xi = 2.7 \times 10^{-2} r_c [\tfrac{1}{16} \times 10^{20} D_{\mathrm{mean}}^4 (1+\nu)^{-0.5} - 0.4], \tag{75}$$

and

$$\tau = \frac{3.7}{\rho_a r_c} [0.5 \times 10^6 D_{\mathrm{mean}} (1+\nu)^{-0.5} - 0.75]^{-1}. \tag{76}$$

In analogy with the application of Eq. (50) to diagnose melting of coalesced hydrometeors and consequent mass conversion to new categories, similar melting conversions are performed for the categories as a whole when Q^* is evaluated in Eq. (22). At this stage in the sequence of computations, the sources and sinks of mass and energy from all other processes have been summed, and any melting of ice categories is diagnosed as resulting from an energy surplus. As done for coalesced hydrometeors, the quotient Q^*/L_{il} is taken as the fraction of liquid in the category. The decisions governing the transfer of mass and energy from ice categories following melting are similar to those made for coalesced hydrometeors, except that no riming or freezing is involved here. Complete melting of ice categories produces rain. Partial melting of snow and aggregates cause some of their mass to be converted to graupel, and partial melting of graupel causes some of its mass to be converted to hail. Individual pristine ice crystals are assumed to melt entirely or not at all. If the diagnosed fraction of liquid is between 0 and 1, that fraction is transferred to rain, while the ice remains in the pristine ice category. The number concentration for pristine ice is reduced in the same proportion as mixing ratio during melting, as is done for collection of pristine ice. Given the small size of pristine ice, complete melting of the category to rain is likely to occur rapidly once melting begins. We compute the mixing ratio of ice transferred to the secondary category by

$$\Delta r_{\mathrm{it}} = 2 r_{\mathrm{i}} \left(\frac{Q^*}{L_{\mathrm{il}}} \right), \tag{77}$$

based on the reasoning that an amount of melt water produced will convert an equal amount of ice to a more dense structure, and together they should be recategorized. This formula is experimental.

Although the hail category is permitted to contain liquid, excess liquid is shed to the rain category. The amount shed is based on a formula proposed by Rasmussen et al. (1984) for the maximum liquid water mass m_{l} that can be retained by an ice core of mass m_{i}, which in units of grams is given by

$$m_{l,max} = 0.268 \times 10^{-3} + 0.1389 m_i. \quad (78)$$

It would be possible to integrate this formula over the entire hail distribution to obtain a maximum allowable value of liquid to mass ratio for the category, and shed when the category liquid content exceeds this value. However, there are physical situations where, due to differential melting and liquid collection rates with hail size, some hail sizes will be below the threshold for shedding while others will exceed it; thus, this effort seems unwarranted. Furthermore, other authors (e.g., Chong and Chen, 1974) have observed significantly different liquid water retention amounts. We therefore take the simple approach of applying Eq. (78) directly to the mean mass $\overline{m}$ of the hail distribution, and shedding when the fractional liquid water content exceeds the maximum allowed for that mass.

2.8. Sedimentation

Gravitational settling of hydrometeors causes them to fall relative to air. Since transport of hydrometeors due to resolved and subgrid air motions in the model is evaluated elsewhere (see Eq. 12), sedimentation only deals with the mass-weighted relative fall velocity between the hydrometeor and air, which is given by Eq. (9). We first evaluate Eq. (12) without the SEDIM(r) term, and update mixing ratio r based on all other terms. Sedimentation is then carried out on the updated r to obtain a final value for the timestep.

A Lagrangian scheme is used to transport the mixing ratio from any given grid cell to a lower height in the vertical column. Before sedimentation, the mixing ratio is identified as a collection of volumes each corresponding to a grid cell bounded by a top height z_{top} and bottom height z_{bot}. The volume is assumed to fall at speed $\overline{v}_t$ for the timestep, resulting in new heights of the top and bottom surfaces of the volume given by

$$z_{topnew} = z_{top} - \overline{v}_t \Delta t, \quad (79)$$

and

$$z_{botnew} = z_{bot} - \overline{v}_t \Delta_t. \quad (80)$$

We then identify which grid cell or cells are overlapped by the displaced volume, and in what proportion. The mixing ratio is transferred from the original grid cell to the new ones in the given proportions. This scheme allows sedimentation which is more rapid than one grid level per timestep (a limiting velocity of Eulerian methods), which can often occur when vertical grid stretching is used to provide high resolution near the ground.

In evaluating the SEDIM term for number concentration for pristine ice, we currently transport N_t in the same proportion as mixing ratio. However, we are developing a sedimentation scheme which allows differential fall speeds of both mass and number as a function of D to be applied in cases where number is prognosed for all species.

3. Model tests

In this section we present results of numerical simulations with RAMS using the new microphysics package. The primary purpose of these experiments is to demonstrate model

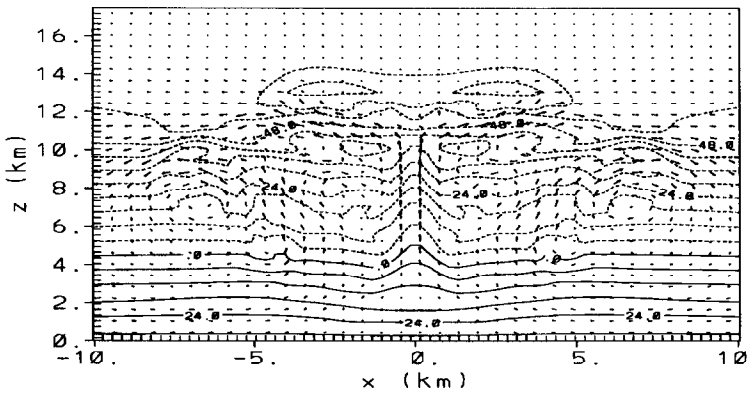

Fig. 2. Experiment 1 temperature and vector velocity fields at 15 minutes. Temperature contour interval is 6°C, and maximum length vector represents [57 m s^{-1}].

behavior for an idealized (convective) system, and to explore some of the effects that the expanded capabilities of the model can have on model solutions. For example, introduction of the generalized gamma distributions for all categories allows a much greater diversity of hydrometeor spectra than the former use of only Marshall–Palmer distributions. In addition, we vary a few other selected parameters and examine their effects.

These simulations are not intended as a verification of the microphysical model, except to point out that the microphysical, temperature and velocity fields, and precipitation amounts, are within physically-expected limits for the given atmospheric environment. Verification of the model against observations, in the form of case studies of orographic precipitation over the Colorado Rockies and a supercell storm, are currently being conducted with the new scheme, and will be reported elsewhere. In those studies, observations of shape parameters and mean diameters of hydrometeor categories are generally unavailable. For this reason, and because, as demonstrated below, the simulation results are often sensitive to specified microphysical parameters, verification must include comparisons of observed features such as precipitation amount, location, and time, against the model for several different parameter settings.

For simplicity, we perform idealized simulations in a two-dimensional computational domain over flat terrain, with no surface fluxes of heat or moisture. A deep convective cell is simulated, which is expected to produce large amounts of both liquid and ice. A computational domain 24 km deep and 60 km in horizontal extent is used, with grid spacing of 300 m both horizontally and vertically. Initial conditions consist of zero winds, temperatures of 306 K and 218 K at the surface and 11 km, respectively, with a constant lapse rate between and constant temperature above, and a water vapor mixing ratio of 15 g kg^{-1} below 2 km and very dry air above 3 km. A Rayleigh friction absorbing layer is used above 18 km to damp gravity waves and prevent their reflection off the upper rigid lid. Convection is initiated by a 5-km-wide bubble of temperature 5 K warmer warmer and 2 g kg^{-1} moister than the environment, horizontally-centered in the domain in the lowest 3 km.

In all experiments, we prognose N_t for pristine ice, specify N_t for cloud droplets, and specify $D_{\overline{m}}$ for all other categories. We define a control experiment, denoted by Experiment

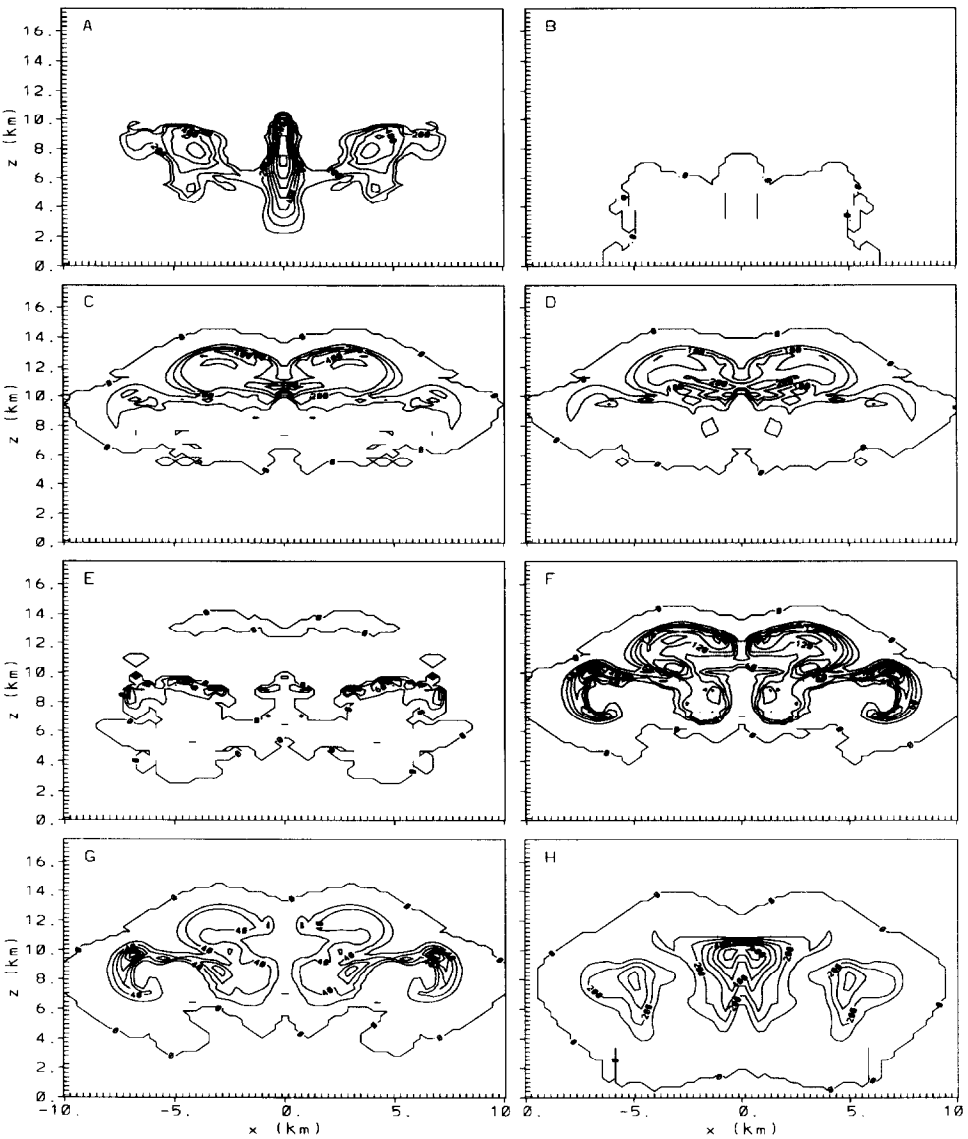

Fig. 3. Experiment 1 microphysical fields at 15 minutes. Contour intervals shown in brackets. Units are [g kg^{-1}] for mixing ratios: (A) r_c [1.0], (B) r_r [0.5], (C) r_p [1.0], (D) N_t for pristine ice [50000 l^{-1}], (E) r_s [0.003], (F) r_a [0.3], (G) r_g [0.2], (H) r_h [1.0].

1, in which the shape parameter ν is set to 1 (the Marshall–Palmer distribution) for all categories, $N_t = 300\,\mathrm{cm}^{-3}$ for cloud droplets, and $D_{\overline{m}} = 0.1$ cm for the rain, snow, aggregate, and graupel categories, and 0.3 cm for the hail category. Three additional experiments are performed, numbered 2 to 4, in which one parameter is set different from the control case.

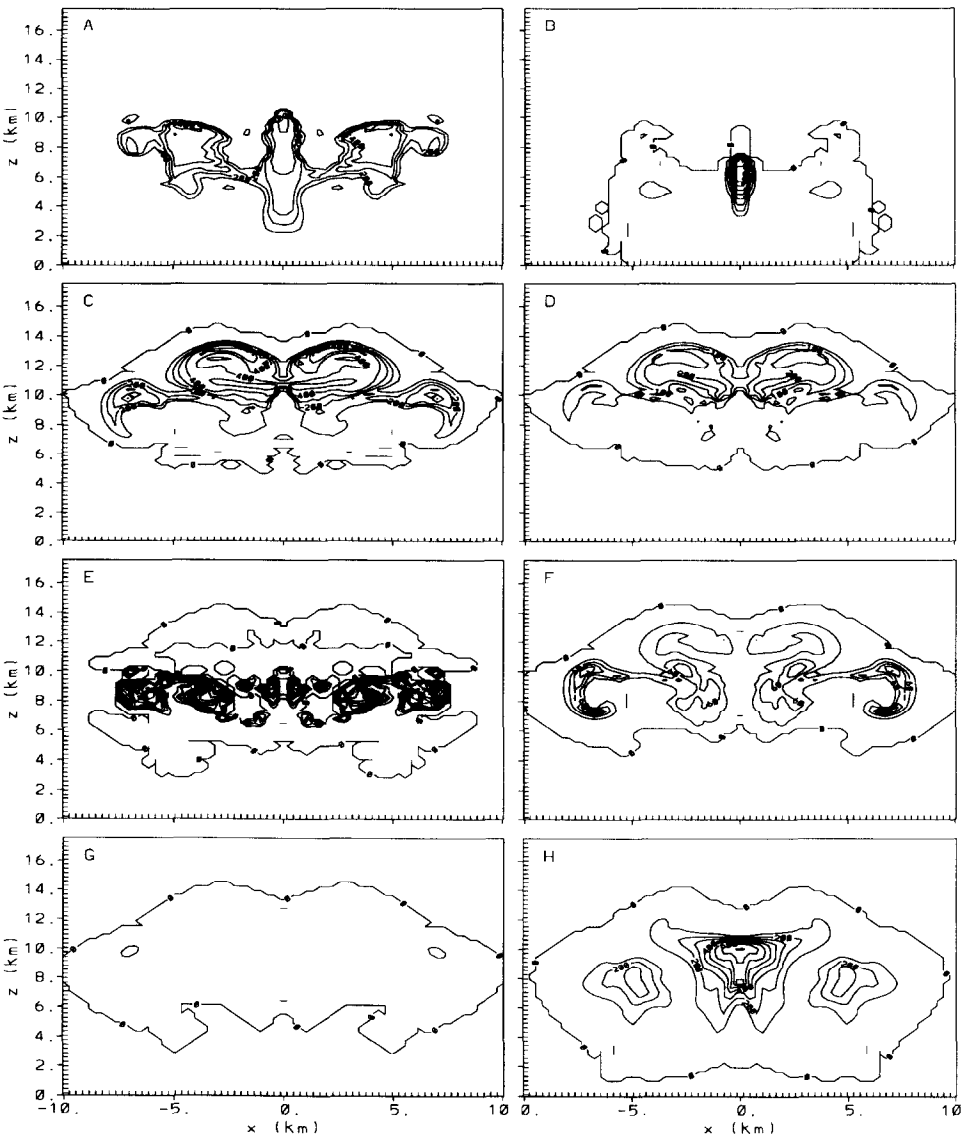

Fig. 4. Experiment two microphysical fields at 15 min. Contour intervals are identical with corresponding fields of Fig. 3. (A) r_c, (B) r_r, (C) r_p, (D) N_t for pristine ice, (E) r_s, (F) r_a, (G) r_g, (H) r_h.

Convective motion develops nearly identically in the first 15 to 20 min for all experiments. It is dominated by the initial warm bubble in the first few minutes, and by latent heat release for many minutes afterward. The updraft velocity reaches a maximum strength of about 55 m s^{-1}, between 15 and 20 min, and then weakens due to significant precipitation loading in the updraft location, plus reduced convective instability. Fig. 2 shows the vector velocity and temperature fields at 15 min for Experiment 1. The central updraft is evident, as is a

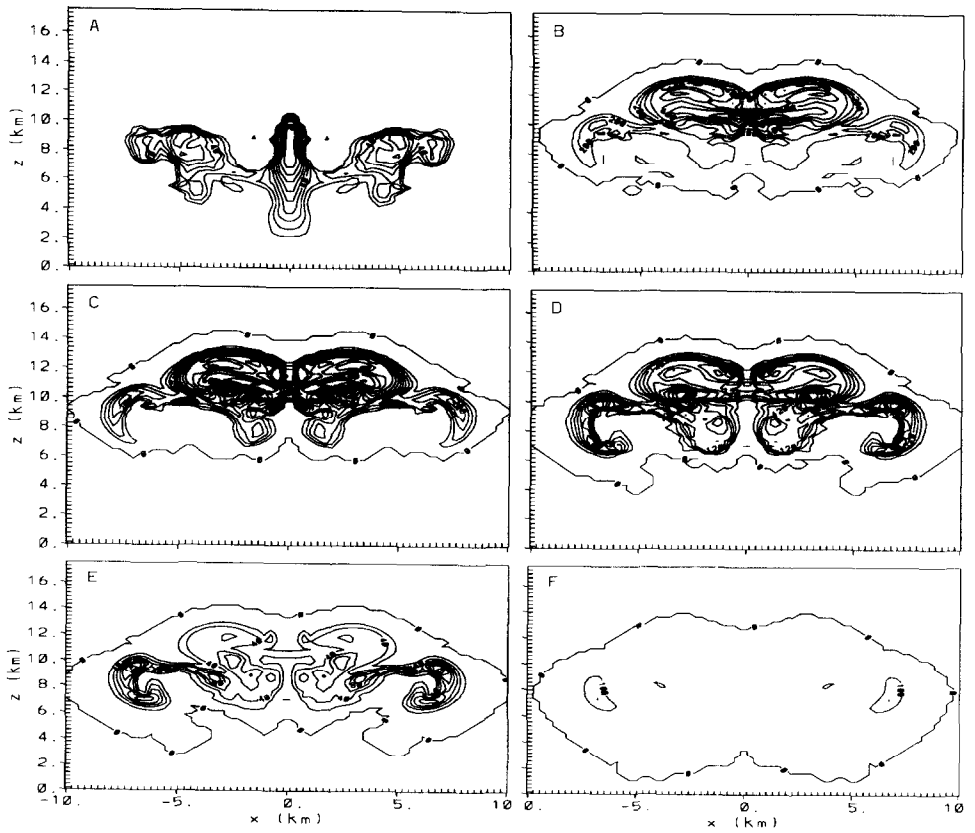

Fig. 5. Experiment 3 microphysical fields at 15 min. Contour intervals are identical with corresponding fields of Fig. 3. (A) r_c, (B) r_p, (C) N_i for pristine ice, (D) r_a, (E) r_g, (F) r_h.

collocated warm temperature perturbation resulting from latent heat release. Secondary, weaker updrafts and temperature maxima have developed around 5 km away on either side due to propagating gravity waves from the initial convective pulse in the center. Strong horizontal flow away from the updrafts occurs near tropopause level. The freezing level is slightly above 4 km, although near 5 km in the central updraft. The velocity and temperature fields are nearly identical at this time for all other experiments, and are thus not shown. At 30 min, the main updraft has disappeared or substantially weakened in all experiments, and considerable variation exists between the velocity fields. In contrasting microphysical fields between experiments, we thus concentrate on the time of 15 min so that differences are not a result of differing kinematics. At this relatively early time in the simulation, the larger hydrometeor categories have not been in existence long, and no significant precipitation has reached the ground.

Fig. 3 shows the pristine ice crystal concentration, and the mixing ratio fields for cloud water, rain, pristine ice, snow, aggregates, graupel, and hail for Experiment 1. The cloud water field reaches a mixing ratio of 8 g kg^{-1} in the main updraft at a height of 7 km. This large value reflects the rapid condensation of water vapor in the strong updraft, and the

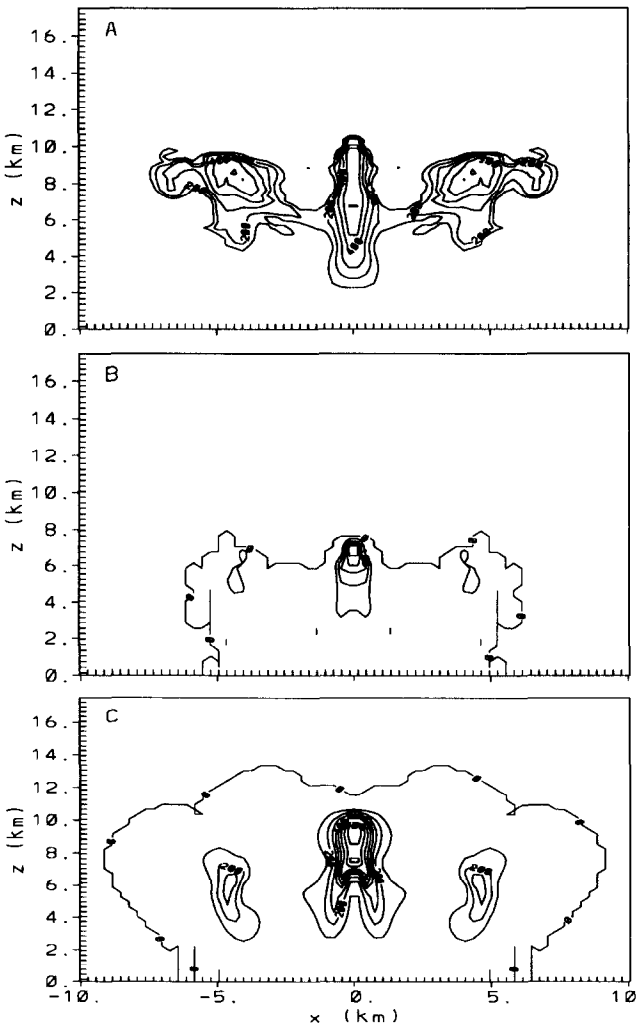

Fig. 6. Experiment 4 microphysical fields at 15 min. Contour intervals are identical with corresponding fields of Fig. 3. (A) r_c, (B) r_r, (C) r_h.

comparative slowness of conversion of cloud water to rain and ice. Weaker maxima in the cloud water field appear in the secondary updrafts. The rain mixing ratio is mostly below 0.5 g kg^{-1}. Pristine ice begins forming above 6 km in the main updraft due to heterogeneous nucleation. Some of these crystals combine to form aggregates, while others collide with rain to form hail. Riming of aggregates produces graupel, and heavy riming of graupel produces additional hail. The result of all these processes is that hail becomes the most abundant hydrometeor mixing ratio in the main updraft after cloud water. The graupel and aggregates fields have a very similar spatial pattern. This largely reflects the previous history of the convection in which cloud water and pristine ice both formed in the single original

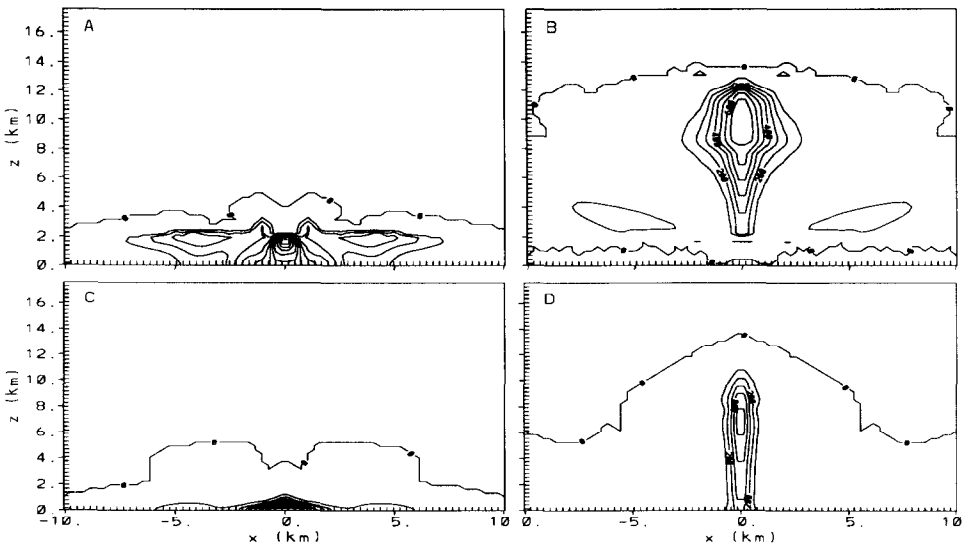

Fig. 7. Rain and hail fields at 25 min. Contour intervals are identical with corresponding fields of Fig. 3. (A) Experiment 1 r_r, (B) Experiment 1 r_h, (C) Experiment 4 r_r, (D) Experiment 4 r_h.

updraft. Graupel and aggregates were both produced in this environment and subsequently advected upward and outward as the flow field evolved.

Near 10 km, where the temperature is close to $-40°C$ (see Fig. 2), homogeneous nucleation of cloud droplets in the updraft occurs, which produces ice mixing ratios exceeding 4 g kg^{-1} and ice crystal concentrations close to 2×10^5 l^{-1}. Such high concentrations result directly from the specified high cloud droplet concentration, and the fact that homogeneous freezing produces one crystal per cloud droplet. In this simulation, it is evident that most pristine ice is produced through homogeneous, rather than heterogeneous, nucleation. The mixing ratio field of aggregates strongly resembles that for pristine ice due to direct

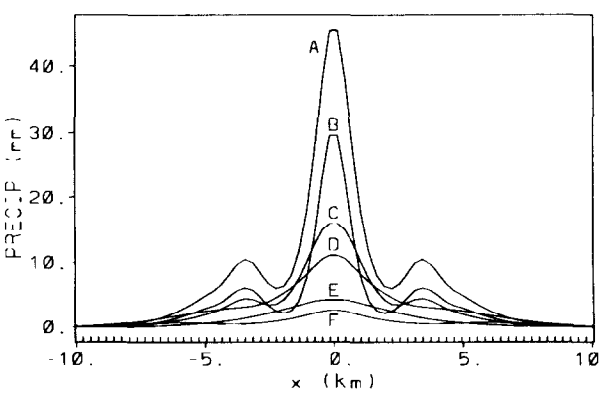

Fig. 8. Accumulated precipitation at 30 min. (A) Experiment 4 total, (B) Experiment 4 hail, (C) Experiment 4 rain, (D) Experiment 1 total, (E) Experiment 2 total, (F) Experiment 3 total.

conversion by coalescence, and with values reaching 2 g kg^{-1}, aggregates represent a significant sink of pristine ice.

The amount of snow forming is quite small, mainly because considerable time is required for an ice crystal to grow by vapor diffusion to the larger size of snow, and because rapidly rising parcels soon undergo homogeneous freezing of cloud water where ice crystals become so numerous that they strongly compete for vapor. Most of the snow is found below the homogeneous freezing level, where there are relatively few pristine ice crystals, and in the weaker secondary updrafts where there is presumably more time for the larger crystals to form during ascent while vapor is abundant. (We mention here that in simulations of gradual orographic lifting performed elsewhere with this model, snow mixing ratios comparable with pristine ice have been produced.)

Experiment 2 differs from the control in that it uses a gamma distribution for all categories with $\nu = 3$. When changing this parameter, one will implicitly change all moments of the distribution except for at most one. We have chosen the mean mass (third moment) as the moment to hold constant for rain, snow, aggregates, graupel, and hail, so that the ratio of mixing ratio to number concentration will be unchanged. This implies that the characteristic diameter D_n is altered for these categories. For cloud water, we hold number concentration constant, so that the ratio of mixing ratio to mean mass will be unchanged. This seems the most logical way to examine the results of changes in the shape parameter ν.

Fig. 4 shows the set of fields for Experiment 2 corresponding to the Experiment 1 fields in Fig. 3. A basic difference is that conversion of cloud water to rain within the central updraft is more rapid, resulting in a greatly reduced cloud water mixing ratio above 4 km, and a corresponding increase in rain up to 4 g kg^{-1}. Note that in increasing the shape parameter from 1 to 3, for a given $\overline{m}$, the mean diameter D_{mean} for cloud water is increased by about 40%. The autoconversion rate increases sharply with D_{mean} (Berry and Reinhardt, 1974).

One consequence of the large rain production is that conversion of rain (coalescing with ice) to hail is much more rapid in the updraft between 6 and 8 km; the hail mixing ratio is nearly doubled at 8 km compared with Experiment 1. This conversion also depletes the rain, which disappears above 8 km. Continued conversion of cloud water to hail is greatly reduced above 8 km in contrast to Experiment 1, however, so the resulting hail mixing ratios at 10 km in the main updraft are very similar. A second consequence is that the reduced cloud water below the homogeneous freezing level causes less riming of snow and aggregates to produce graupel, whose mixing ratios are well below those of Experiment 1. Snow appears in Experiment 2 at several times the mixing ratio of Experiment 1, but the amount present is still much smaller than other categories. Possibly reduced collisions with graupel are responsible for the greater snow present.

At the homogeneous freezing level (10 km), Experiment 2 has somewhat less cloud water remaining in the central updraft than Experiment 1, and thus less pristine ice is produced above. However, more pristine ice coalesces into aggregates in Experiment 1, so the remaining pristine ice mixing ratios and number concentrations are similar in the two cases. The reduced aggregation is in part a direct consequence of the higher shape parameter, which decreases the spectral width of the pristine ice and makes its fall velocities more uniform.

Experiment 3 is identical to Experiment 1 except that N_t of cloud droplets is increased to 1000 cm^{-3} as if the environment contains dirtier continental air. Selected results are shown in Fig. 5. The most immediate consequence of large cloud droplet concentration is a reduced droplet diameter, and a greatly reduced conversion of cloud water to rain. There is in fact virtually no rain present in the simulation at 15 min, and the field is therefore not shown. In the central updraft below the homogeneous freezing level, nearly all condensate remains as cloud water, resulting in cloud water mixing ratios reaching 9 g kg^{-1}. An abrupt conversion to pristine ice occurs immediately above, and produces an equivalent ice mixing ratio. The ice crystal concentration is, as would be expected, about triple the previous value, resulting directly from homogeneous nucleation of cloud droplets. Snow (not shown) is not appreciably affected by the cloud droplet concentration, probably because it develops mostly from ice that has been heterogeneously nucleated, and the development of such ice below the homogeneous freezing level is not dependent on cloud water. Aggregates are more abundant than in Experiment 1 because of the greater supply of pristine ice. Graupel is likewise more abundant, owing largely to the increased aggregates (recall that pristine ice does not rime). Hail is largely absent, however, mainly because of the lack of rain. Thus, the higher number of cloud droplets causes most of the water to remain in the lighter ice categories rather than rain and hail.

In Experiment 4, $D_{\overline{ni}}$ of hail is increased to 1 cm, but all other parameters are identical with the control case. Selected results at 15 min are given in Fig. 6. The larger hail has almost no effect on the lighter ice categories compared with Experiment 1, and these are thus not shown. Because of its greater fall speed, significant hail extends downward to 3 km, compared with 5 km in Experiment 1 in sedimentation lobes either side of the central updraft, and likewise extends lower within the updraft. This is well below the freezing level, and some of the hail consequently melts to rain. The rain falls more slowly, and is thus carried upward in the updraft. Production of additional rain becomes significant in the updraft due to collection of cloud droplets, and consequently more rain plus less cloud water results in comparison with Experiment 1.

At 25 min, precipitation is close to maximum intensity in all experiments, but the amounts differ widely. Fig. 7 compares the rain and hail mixing ratio fields between Experiments 1 and 4, which produce the most surface precipitation. Hail is concentrated mainly in the center in both cases, although the hail shaft is particularly narrow in Experiment 4, while mixing ratios over 1 g kg^{-1} occur over a 15 km wide band in Experiment 1. The much larger hail diameter in Experiment 4, which causes higher fall velocities, is largely responsible for this difference. The higher fall velocity has also caused most of the hail to have fallen out of the air by this time, leading to the lower total hail amount in Experiment 4, while both the higher velocity and larger hail diameter cause most of the hail to reach the ground without melting in Experiment 4, in contrast to Experiment 1. The rain in both experiments is almost entirely contained below 3 km, and is produced almost entirely by hail melting and shedding below the freezing level. Because of the slower melting rate of the large hail in Experiment 4, rain is confined even closer to the surface.

Fig. 8 compares the total accumulation of precipitation at the surface for all Experiments at 30 min by which time precipitation has slowed. Approximately 1 cm has fallen in the center region in Experiment 1, all in the form of rain, while Experiment 2 has produced about half this amount. This is mostly due to the fact that Experiment 2 has considerably

more pristine ice remaining in the upper atmosphere than all other Experiments, a result of a reduced aggregation rate owing to the narrower spectral width of ice for this case. Experiment 3 has the greatest mass remaining as aggregates of all cases, plus the greatest combined mass of pristine ice, snow, aggregates and graupel. As mentioned above, the higher cloud droplet concentration for this case inhibited the conversion to rain and consequently to hail. Consequently, Experiment 3 has the lowest precipitation total of all cases. Experiment 4 has by far the greatest surface accumulation at 30 min, and is the only case to have any hail reaching the surface. The sum of remaining pristine ice, snow, aggregates, and graupel mass for this case is intermediate between Experiments 1 and 2. The high total precipitation at the surface is mainly due to the fact that nearly all rain and hail have fallen by this time, while in Experiments 1 and 2, much remains in the atmosphere.

4. Summary

The microphysical parameterization presented in this paper represents a collection of several new technological advancements, and a culmination of a long history of research and development. New features include: – Use of generalized gamma distributions for all hydrometeor categories – Introduction of separate graupel and hail categories which allow both liquid and ice phases – A double spectrum for the representation of ice crystals, allowing a bi-modal spectrum to develop if dictated by the model physics – Implementation of new parameterizations of homogeneous nucleation of ice from haze and cloud water – Use of the stochastic collection equation for all hydrometeor collisions other than autoconversion of cloud water, and an efficient table lookup of collection integral values – Solution of hydrometeor heat budget equations which include sensible heat transfer in inter-species collisions

The initial sensitivity tests reported here demonstrate physically plausible results and responses to changes in input parameters. A wide range of additional tests are to be carried out, with comparisons against data gathered from a number of field programs, as well as comparisons with explicit bin model calculations. The model is intended to serve as a major tool to support basic research on convective storms and mesoscale convective systems, cirrus clouds, and stratocumulus clouds, as well as applied research in mesoscale forecasting of clouds, precipitation, ceilings, and visibility.

Acknowledgements

This research was supported under National Science Foundation grant #ATM-9118963, DOD, Office of Scientific Research, Grants #F49620-92-J-0331M and AFOSR-91-0269, and the National Oceanic and Atmospheric Administration under contract #NA90RAH-00077. Ms. Brenda Thompson assisted in preparation of the manuscript. We are particularly indebted to Hans Verlinde and Piotr Flatau for their many contributions to the development of the new scheme, and to Paul DeMott for his contributions to the development of the nucleation parameterizations.

References

Arnott, W.P., Dong, Y.Y. and Hallett, J., 1993. Cirrus microphysics observations made during FIRE II: Small particles, high concentrations, and probe comparisons. Preprints, FIRE Cirrus Science Conf., June 14–17, 1993, Breckenridge, Colorado, pp. 5–8.

Berry, E.X. and Reinhardt, R.L., 1974. An analysis of cloud drop growth by collection: Part IV. A New Parameterization. J. Atmos. Sci., 31: 2127–2135.

Chong, S. and Chen, C., 1974. Water shells on ice pellets and hailstones. J. Atmos. Sci., 31: 1384–1391.

Cotton, W.R., 1972a. Numerical simulation of precipitation development in supercooled cumuli, Part I. Mon. Weather Rev., 100: 757–763.

Cotton, W.R., 1972b. Numerical simulation of precipitation development in supercooled cumuli, Part II. Mon. Weather Rev., 100: 764–784.

Cotton, W.R., Stephens, M.A., Nehrkorn, T. and Tripoli, G.J., 1982. The Colorado State University three-dimensional cloud/mesoscale model — 1982. Part II: An ice-phase parameterization. J. Rech. Atmos., 16: 295–320.

Cotton, W.R., Tripoli, G.J., Rauber, R.M. and Mulvihill, E.A., 1986. Numerical simulation of the effects of varying ice crystal nucleation rates and aggregation processes on orographic snowfall. J. Clim. Appl. Meteorol., 25: 1658–1680.

DeMott, P.J., Meyers, M.P. and Cotton, W.R., 1994. Parameterization and impact of ice initiation processes relevant to numerical model simulations of cirrus clouds. J. Atmos. Sci., 51: 77–90.

Ferrier, B.S., 1993. A double-moment multiple-phase four-class bulk ice scheme. Part I: Description. J. Atmos. Sci., 51: 249–280.

Flatau, P.J., Tripoli, G.J., Verlinde, J. and Cotton, W.R., 1989. The CSU-RAMS Cloud Microphysical Module: General Theory and Code Documentation. Colorado State Univ., Dep. Atmos. Sci., Fort Collins, Colorado 80523. Atmos. Sci. Pap., 451, 88 pp.

Flatau, P.J., Walko, R.L. and Cotton, W.R., 1992. Polynomial fits to saturation vapor pressure. J. Appl. Meteorol., 31: 1507–1513.

Harrington, J.L., 1994. Parameterization of ice crystal conversion process in cirrus clouds using double-moment basis functions. M.S. Thesis, Colorado State Univ., Dep. Atmos. Sci., Fort Collins, CO 80523, in prep.

Harrington, J.L., Cotton, W.R., Meyers, M.P. and Walko, R.L., 1995. Parameterization of ice crystal conversion processes due to vapor deposition for mesoscale models using double moment basis functions. Basic formulation and parcel model results. J. Atmos. Sci., accepted.

Kessler, E., III, 1969. On the Distribution and Continuity of Water Substance in Atmospheric Circulation. Meteorol. Monogr., Am. Meteorol. Soc., 84 pp.

Koenig, L.R., 1977. The rime-splintering hypothesis of cumulus glaciation examined using a field-of-flow cloud model. Q. J. R. Meteorol. Soc., 103: 585–606.

Lavoie, R.L., Cotton, W.R. and Hovermale, J.B., 1970. Investigations of Lake Effect Storms. Final Rep. Environ. Sci. Serv. Administration, Boulder, CO, Contract No. E22-103-68(N), January 1970, 127 pp.

Marshall, J.S. and Palmer, W.M., 1948. The distribution of raindrops with size. J. Meteorol., 5: 165–166.

Meyers, M.P., DeMott, P.J. and Cotton, W.R., 1992. New primary ice nucleation parameterizations in an explicit cloud model. J. Appl. Meteorol., 31: 708–721.

Meyers et al., 1995. New RAMS Cloud microphysics parameterization. Part II: The two-moment prediction scheme. Submitted to Atmos. Res.

Mitchell, D.L., Chai, S.K., Dong, Y., Arnott, W.P., Hallett, J. and Heymsfield, A.J., 1993. Importance of aggregation and small ice crystals in cirrus clouds, based on observations and an ice particle growth model. Preprints, FIRE Cirrus Science Conf., June 14–17, 1993, Breckenridge, Colorado, pp. 159–162.

Nickerson, E.C., Fritsch, J.M., Chappell, C.F. and Smith, D.R., 1978. Numerical Simulations of Orographic and Convective Cloud Systems. Annu. Rep. U.S. Dep. Interior, Bureau of Reclamation, Eng. Res. Ctr., Denver, CO, Contract #8-07-83-V0017, 114 pp.

Nickerson, E.C., Richard, E., Rosset, R. and Smith, D.R., 1986. The numerical simulation of clouds, rain, and airflow over the Vosges and Black Forest Mountains: A meso-β model with parameterized microphysics. Mon. Weather Rev., 114: 398–414.

Orville, H.D. and Kopp, F.J., 1977. Numerical simulation of the life history of a hailstorm. J. Atmos. Sci., 34: 1596–1618.

Pruppacher, H.R. and Klett, J.D., 1978. Microphysics of Clouds and Precipitation. Reidel, Boston, 714 pp.

Rasmussen, R.M., Levizzani, V. and Pruppacher, H.R., 1984. A wind tunnel and theoretical study on the melting behavior of atmospheric ice particles. III: Experiment and theory for spherical ice particles of radius >500 μm. J. Atmos. Sci., 41: 381–388.

Simpson, J. and Wiggert, V., 1969. Models of precipitating cumulus towers. Mon. Weather Rev., 97: 471–489.

Srivastava, R.C. and Coen, J.L., 1992. New explicit equations for the accurate calculation of the growth and evaporation of hydrometeors by the diffusion of water vapor. J. Atmos. Sci., 49: 1643–1650.

Tripoli, G.J. and Cotton, W.R., 1981. The use of ice–liquid water potential temperature as a thermodynamic variable in deep atmospheric models. Mon. Weather Rev., 109: 1094–1102.

Verlinde, J., Flatau, P.J. and Cotton, W.R., 1990. Analytical solutions to the collection growth equation: Comparison with approximate methods and application to cloud microphysics parameterization schemes. J. Atmos. Sci., 47: 2871–2880.

Wang, C. and Chang, J., 1993. A three dimensional numerical model of cloud dynamics, microphysics, and chemistry 1. Concepts and formulations. J. Geophys. Res., 98: 14827–14844.

Weinstein, A.I., 1970. A numerical model of cumulus dynamics and microphysics. J. Atmos. Sci., 27: 246–255.

Weinstein, A.I. and Davis, L.G., 1968. A Parameterized Numerical Model of Cumulus Convection. Rep. II, NSF GA-777, 43, Natl. Sci. Foundation, Washington, DC, 43 pp.

Wisner, C., Orville, H.D. and Myers, C., 1972. A numerical model of a hail-bearing cloud. J. Atmos. Sci., 29: 1160–1181.

Ziegler, C.L., 1985. Retrieval of thermal and microphysical variables in observed convective storms. Part I: Model development and preliminary testing. J. Atmos. Sci., 42: 1487–1509.